

Communication

Effect of Contact Angle on Friction Properties of Superhydrophobic Nickel Surface

Junyuan Huang ^{1,†}, Zhiwei Zhu ^{2,†}, Ling Zhang ^{3,4,*}, Dongdong Guo ⁵, Zhen Niu ⁵ and Wei Zhang ^{1,*}

¹ School of Mechanical Engineering and Automation, Beihang University, Beijing 100191, China; jyhuang@buaa.edu.cn

² Department of Mechanical and Automation Engineering, The Chinese University of Hong Kong, Hong Kong, China; zhiweizhu@cuhk.edu.hk

³ Key Lab of Semiconductor Materials Science, Institute of Semiconductors, Chinese Academy of Sciences, Beijing 100083, China

⁴ Joint Lab of Digital Optical Chip, Wuyi University, Jiangmen 529020, China

⁵ MRA2 Bodyshop, Beijing Benz Automotive Co., Ltd., Beijing 100176, China; guodd@bbac.com.cn (D.G.); niuzhen@bbac.com.cn (Z.N.)

* Correspondence: zhangling@semi.ac.cn (L.Z.); zhangweibh@buaa.edu.cn (W.Z.)

† These authors contributed equally to this work.

Abstract: Due to their excellent performance, superhydrophobic materials have received a lot of attention and research in friction reduction and wear resistance. However, the effect of different contact angles of superhydrophobicity on friction and wear properties has not been thoroughly studied. In this paper, a nanosecond pulsed laser was used to realize the preparation of a superhydrophobic nickel surface, which indeed reduced the coefficient of friction but also increased the wear volume when compared to the unprocessed surface. As the contact angle of the superhydrophobic nickel surface increased, the coefficient of friction gradually increased, and the wear volume decreased gradually in superhydrophobic nickel surfaces. When the laser energy density was 1 J/cm², the contact angle was 150.3° and the minimum friction coefficient was 0.4. However, when the laser energy density was 50 J/cm², the maximum contact angle was 156.4° and the minimum wear volume was 4.23 × 10⁷ μm³. The friction direction also influenced the tribological properties of the superhydrophobic-textured surface. This method makes it possible to process superhydrophobic surfaces with more suitable friction and wear properties.

Keywords: laser surface texturing; nickel; superhydrophobicity; tribology; contact angle



Citation: Huang, J.; Zhu, Z.; Zhang, L.; Guo, D.; Niu, Z.; Zhang, W. Effect of Contact Angle on Friction

Properties of Superhydrophobic Nickel Surface. *Photonics* **2023**, *10*, 829. <https://doi.org/10.3390/photonics10070829>

Received: 20 June 2023

Revised: 6 July 2023

Accepted: 14 July 2023

Published: 17 July 2023



Copyright: © 2023 by the authors. Licensee MDPI, Basel, Switzerland. This article is an open access article distributed under the terms and conditions of the Creative Commons Attribution (CC BY) license (<https://creativecommons.org/licenses/by/4.0/>).

1. Introduction

Wettability is an important characteristic of solid surfaces, and the contact angle is the most used parameter to characterize wettability [1]. The material is superhydrophobic when the water droplet contact angle is greater than 150° and the water droplet sliding angle is less than or equal to 10° [2]. Studies have shown that hydrophobicity can change the properties of the material surface by changing the chemical composition of the material surface and the geometry of the micro/nanostructure, making superhydrophobic materials useful [3,4].

At present, methods for preparing superhydrophobic surfaces on metals include hydrothermal [5], chemical deposition [6], electrodeposition [7], etc. Compared with other superhydrophobic surface fabrication methods, the operation process of laser surface texturing is simple, non-toxic, non-polluting, and has high stability and diversity of processed materials [8,9]. Many studies have discussed laser preparation of superhydrophobic metal surfaces. Rajab [10] obtained a stable superhydrophobic surface on 316 L stainless steel using laser surface texturing. Huang [11] fabricated a superhydrophobic surface on aluminum alloy using laser treatment coupled with a chemical functionalization method.

Lu [12] illustrated that the laser-textured superhydrophobic surface enhanced the corrosion resistance dramatically. Shimada [13] proposed a concept of direct laser processing of two-scale periodic structures exhibiting superhydrophobicity, with the maximum apparent contact angle of 161.4° and the contact angle hysteresis of 4.2° for a pitch of $80\ \mu\text{m}$ and 20 repetition shots. Huang [14] used an ultrafast femtosecond laser to prepare a superhydrophobic/superlipophilic lead bronze surface and found that the anisotropy of the surface structure led to the anisotropy of the tribological properties.

Due to their excellent performance, superhydrophobic materials have good performance in anti-friction [15], anti-corrosion [16], antibacterial [17], etc., and are widely used in aerospace, petroleum engineering, and other fields. Among them, anti-friction and anti-wear have received a lot of attention and research. Jiao [18] manufactured a superhydrophobic aluminum surface with great wear-resistance and decreased the friction force of the sliding interface. Guo [19] carried out nanosecond laser processing to construct a grid of microgrooves on an aluminum surface and reported whether it was under dry friction or water lubrication conditions, with the obtained superhydrophobic samples resulting in good anti-friction and wear-resistant ability. However, the influence of different contact angles of superhydrophobicity on the friction and wear properties has not been thoroughly studied. It is still unknown how large the contact angle of the metal surface can be prepared to have the best tribological properties.

In this paper, the common nickel was used to prepare a nickel surface with superhydrophobic properties by using nanosecond laser processing technology. The effect of laser energy density on wettability was studied, and the friction and wear properties of superhydrophobic surfaces with different contact angles were compared and analyzed. We also analyzed the effect of perpendicular and parallel friction directions on the tribological behavior of superhydrophobic surfaces. This is very important for producing superhydrophobic surfaces with specified tribo-testing directions, which is beneficial for the development of superhydrophobic surfaces with the best contact angle.

2. Experimental Details

2.1. Sample Preparation

The pure nickel content in the nickel material was greater than 99.5%, which was grinded by 800[#], 1000[#], and 1500[#] sandpaper successively to ensure that the roughness of the sample was consistent and smooth before the experiment. And then they were ultrasonic treated with acetone, anhydrous ethanol, and deionized water, respectively, for 5 min and dried with compressed air to remove the impurities on the surfaces. In addition, the above ultrasonic cleaning process was still required after the laser surface texturing for the samples, as shown in Figure 1. The wettability and tribology properties were measured after the samples were exposed to the air for two weeks. In our previous experiments [20], most of the samples achieved superhydrophobicity by exposing nickel to air for two weeks. Of course, the longer the time, the better the superhydrophobicity may be. However, this experiment did not focus on the effect of time on the superhydrophobic properties of the surface, so the performance of the surface of the sample placed at other times was not discussed.

2.2. Laser Surface Texturing

A nanosecond pulsed fiber laser (Sanda laser, YLP-SD20L, Wuhan, China) with 1064 nm center wavelength, 20 kHz repetition frequency, and 10 W maximum average power was adopted in our experiment. The scanning galvanometer with a 110 mm focal length controlled the movement of the laser in the plane, and the focused spot diameter was less than $20\ \mu\text{m}$. The laser processing was carried out in the air with a lateral stripe scanning path. The energy density range could be set from 0 to $100\ \text{J}/\text{cm}^2$ with a scanning interval of 0.5 mm and a scanning speed of 20 mm/s. The experimental principle is shown in Figure 2.



Figure 1. Nickel sample preparation processes.

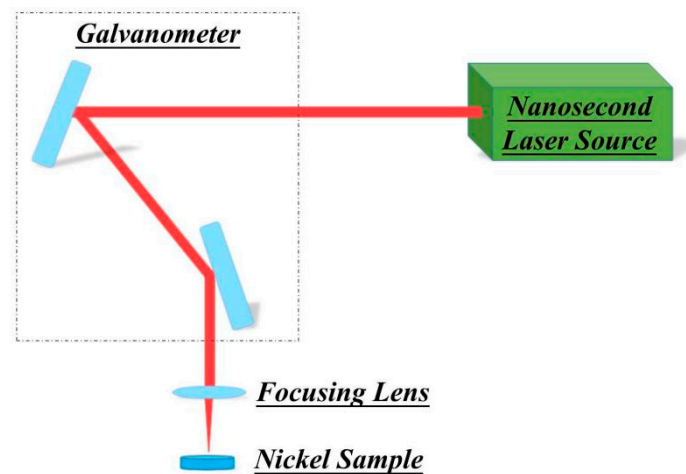


Figure 2. Experimental schematic.

2.3. The Measurement of the Wettability

The water contact angle of the surfaces was measured by the contact angle measuring instrument (OCA20). The surface topography of the samples was observed by the scanning electron microscope (SEM) and the ZYGO NexView white light interferometer (WLI).

2.4. The Antifriction Performance

The SRV-4 friction and wear testing machine was used to analyze the antifriction performance for the point of contact. The friction parts were Si_3N_4 ceramics. The parameters were load of 10 N, time of 20 min, stroke of 1000 mm, and frequency of 20 kHz under dry friction conditions, and each test was repeated three times.

3. Results

3.1. Effect of Laser Energy Density on Contact Angle

According to various laser energy densities, the nickel surface was processed, and the measured contact angle is shown in Figure 3. When the energy density was less than 1 J/cm^2 , the contact angle increased almost linearly with the increase in energy density, from 60.8° on the unprocessed surface to 144.7° at 0.5 J/cm^2 . At this time, the surface had strong adhesion, the surface of the sample was turned over, and the water droplets would not slip off. When the energy density was greater than 1 J/cm^2 , the contact angle showed a stable trend without an obvious increase, and all of them were greater than 150° . The

sample was placed on a platform with an inclination angle of 10° , and the water droplets fell off. Therefore, the samples all exhibited superhydrophobic properties.

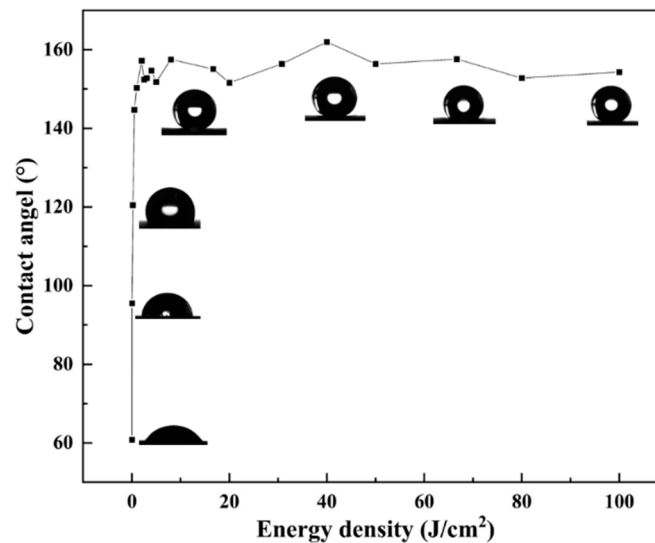


Figure 3. The variation in the water contact angle of the nickel surfaces with the laser energy density.

3.2. Analysis of Wettability Transition Reasons

The surface wettability of materials was mainly related to the surface roughness and surface chemical composition, so the characterization and analysis were carried out for these two aspects. In addition to the unprocessed surface, superhydrophobic samples with laser energy densities of 1, 20, 50, and 100 J/cm² were selected as examples and named U, L1, L20, L50, and L100, respectively.

Figure 4a–e show the SEM two-dimensional topography of samples U, L1, L20, L50, and L100. The two-dimensional diagram showed that the unprocessed surface was very smooth, and the processed superhydrophobic surface formed a periodic stripe structure. Due to the action of the laser, the material in the illuminated area was ablated and removed and then re-solidified in the non-irradiated area. Protrusions were formed on the sample surface due to the rapid temperature drop caused by the movement of the laser beam. These protrusions were attached to a smaller cylindrical protrusion that was spherical and disc-shaped, ranging from a few micrometers to ten micrometers. The striped-textured surface presents a multi-scale micro-nano structure. The formation of these dimples and protrusions increased the surface roughness of the samples [21].

Figure 4f–j show the LCM three-dimensional topography of samples U, L1, L20, L50, and L100. The three-dimensional map and roughness results of the surface roughness after laser processing was much higher than that of the unprocessed surface, and the surface roughness gradually increased with the increase in energy density. According to the roughness results, its relationship with the contact angle was analyzed. The roughness of the superhydrophobic surface was greater than 3564 μm . The surface roughness increased, and the samples also maintain superhydrophobic properties. Therefore, the surface roughness of the samples played an important role in the superhydrophobicity.

Next, the influence of the surface chemical composition on the contact angle was analyzed. The EDS element content map of samples U, L1, L20, L50, and L100 is shown in Figure 5. Since the C content was lower than 1%, the influence of C was ignored. It was considered that the surface contains only O and Ni elements before and after laser processing. The atomic content ratio of each sample is shown in Figure 6. With the increase in the laser energy density, the atomic proportion of O on the surface gradually increased, and the increase rate also gradually decreased, and the change rule was the same as that of the roughness. The change law of the contact angle with the O atom ratio was also similar. An increase in O content represents an increase in the content of metal oxides

formed, and the chemical bonds of metal oxides are polar chemical bonds [22]. The higher the content of polar chemical bonds, the higher the surface free energy, which is not conducive to the acquisition of superhydrophobicity. Considering the surface chemical composition, the increase in laser energy density was not conducive to the formation of surface superhydrophobicity.

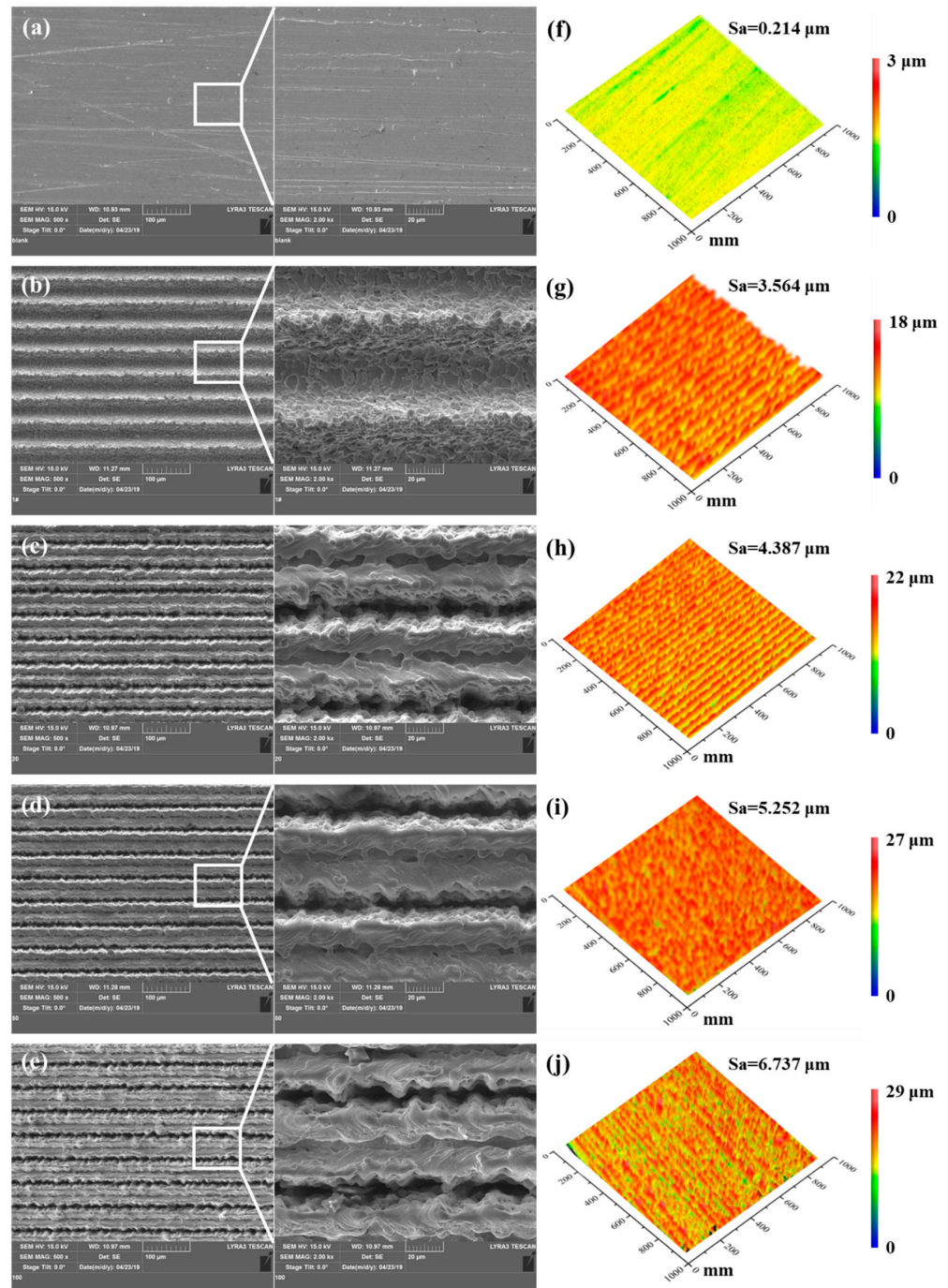


Figure 4. SEM two-dimensional topography and LCM three-dimensional topography of (a) U, (b) L1, (c) L20, (d) L50, and (e) L100. LCM three-dimensional topography of (f) U, (g) L1, (h) L20, (i) L50, and (j) L100.

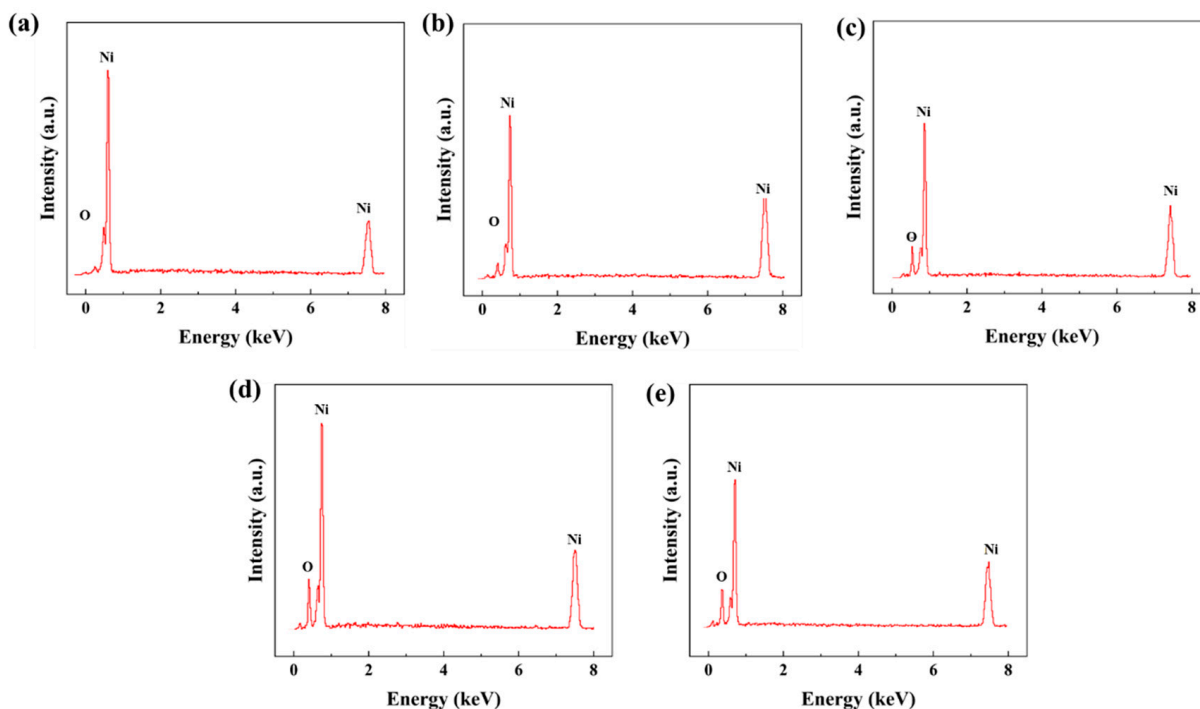


Figure 5. EDS element content diagrams of (a) U, (b) L1, (c) L20, (d) L50, and (e) L100.

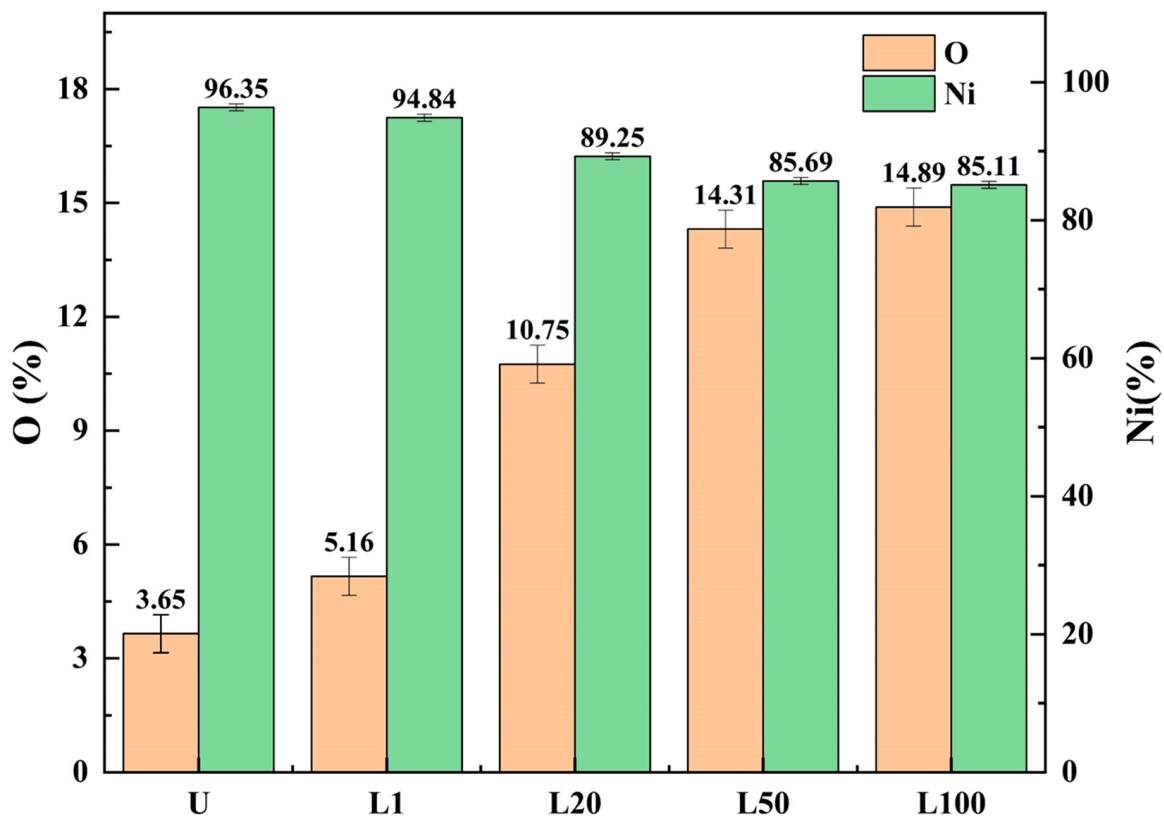


Figure 6. Atomic content ratio of U, L1, L20, L50, and L100.

The above analysis showed that the laser energy density would increase the roughness and O content of the nickel surface at the same time. Under the combined action of the two, the surface with a laser energy density greater than 1 J/cm^2 exhibited superhydrophobic properties. As the energy density increased, the surface roughness increased, which

was conducive to the formation of superhydrophobic surfaces. However, currently, the proportion of O atoms was also increased, and the surface free energy was increased, which was not conducive to the formation of a superhydrophobic surface [23]. Surface roughness played a dominant role at this time, offsetting the adverse effects of surface free energy so that the surface still exhibited superhydrophobic properties. The combined effect of the two also led to the fact that the contact angle did not change monotonously with the increase in surface roughness.

4. Discussion

Next, the effect of laser energy density on the friction and wear properties of superhydrophobic surfaces was analyzed. The superhydrophobic samples with laser energy densities of 1, 20, 50, and 100 J/cm² were still selected for friction and wear experiments. The measured coefficient of friction (COF) curve is shown in Figure 7a. The COF of the superhydrophobic surface was reduced compared with 0.821 of sample U. The relationship between the surface contact angle and the COF was analyzed, as shown in Figure 7b. As the contact angle increased, the COF increased gradually. When the laser energy was 1 J/cm², the contact angle was 150.3° and the minimum friction coefficient was 0.4.

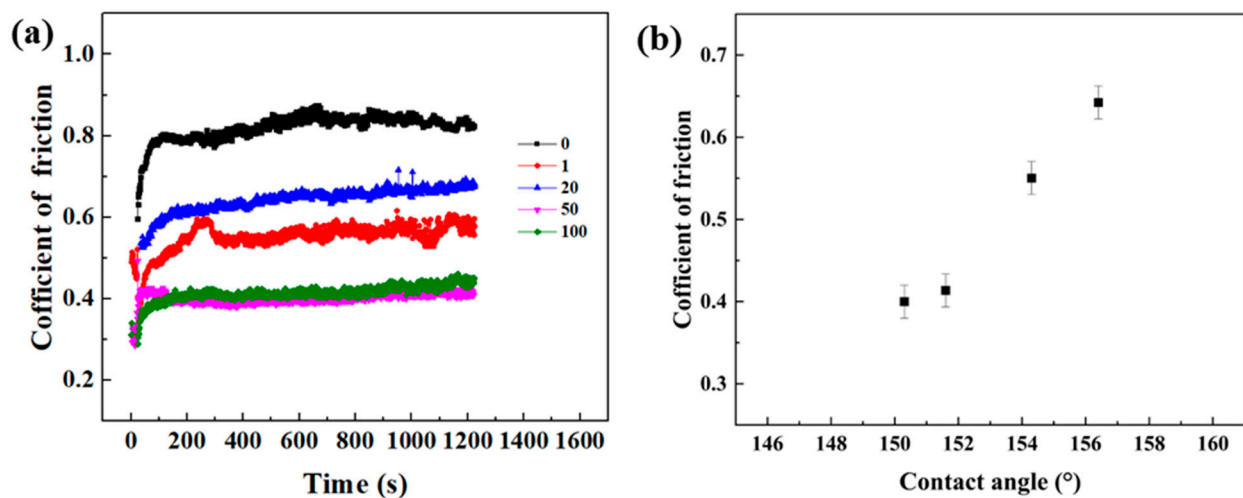


Figure 7. (a) Coefficient of friction (COF) curve. (b) Relationship between the surface contact angle and the COF.

The three-dimensional morphology of the wear scar on the surface after friction is shown in Figure 8. The width of the wear scar on the superhydrophobic surface after laser processing was larger than that of the unprocessed sample U, and the measured wear volume of sample U was $1.25 \times 10^7 \mu\text{m}^3$. The relationship between surface contact angle and wear volume is shown in Figure 9. The wear volume of the superhydrophobic sample surface was larger than that of sample U without processing. With the increase in the contact angle, the wear volume presented a gradually decreasing trend. At 50 J/cm², the maximum contact angle was 156.4° and the minimum wear volume was $4.23 \times 10^7 \mu\text{m}^3$.

The laser-fabricated superhydrophobic surface reduced the COF of nickel but also increased the wear volume. The superhydrophobic property of the surface reduced the adhesion of the surface of the friction pair and reduced the COF. Due to the thermal effect of laser processing, the hardness of the surface micro-nano texture was greater than that of the metal itself. High-hardness abrasive debris would participate in the subsequent friction and wear process, and the resulting ditch effect would increase the wear volume [24]. However, as the contact angle increased, the removal effect of the laser on the material surface increased, the removed surface area increased, and the contact area with the friction piece decreased; therefore, the COF gradually increased [25]. At the same time, when the contact angle increased, the surface roughness also increased. Currently, the surface

micro-nano structure increased, and the surface captured the wear debris, which led to a gradual decrease in the wear volume.

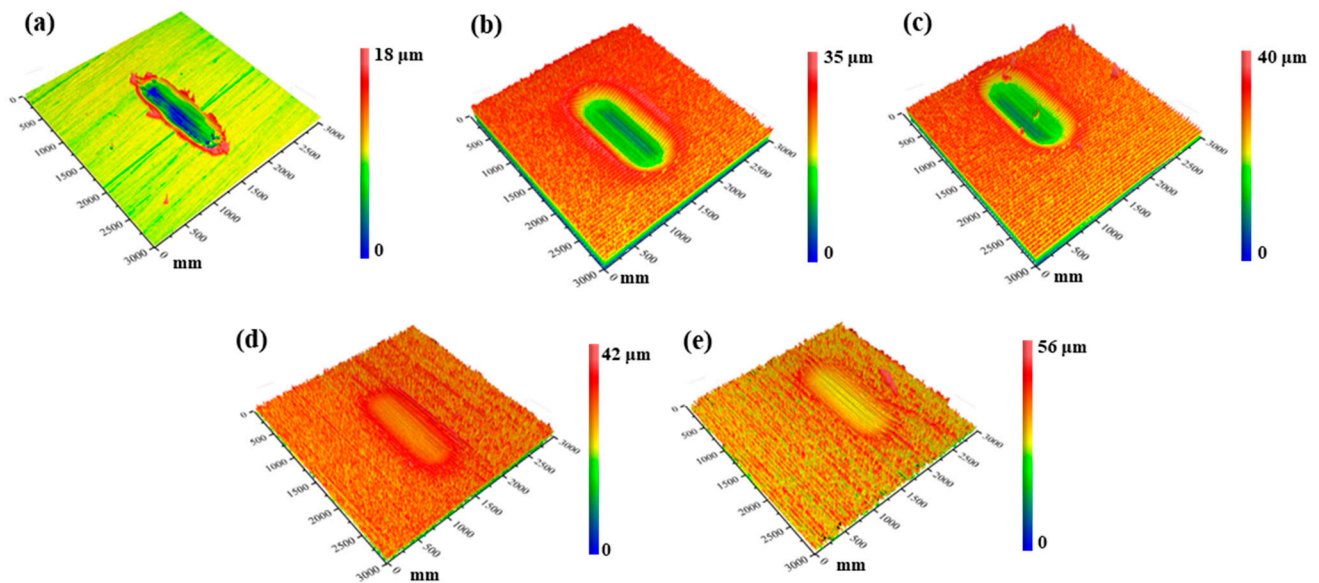


Figure 8. Three-dimensional topography of U and superhydrophobic samples after friction (a) U, (b) L1, (c) L20, (d) L50, and (e) L100.

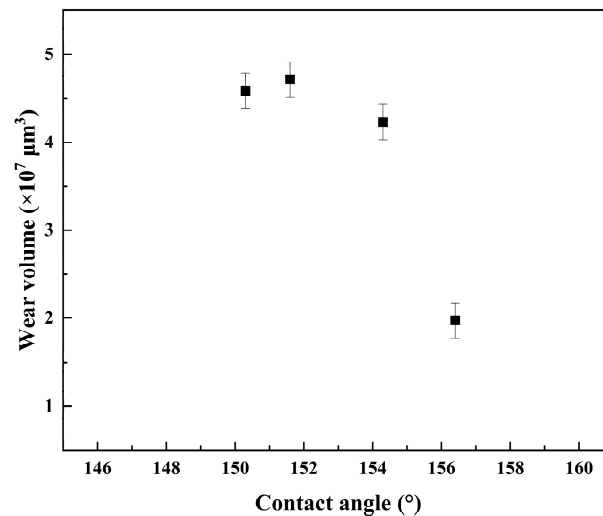


Figure 9. Abrasion volume of U and the superhydrophobic sample surface.

Due to the striped texture, we analyzed the tribological properties of the striped-textured surface in different friction directions. Figure 8 shows that the friction directions of samples L1 and L20 are perpendicular to the stripe texture direction, while the friction directions of L50 and L100 are parallel. It can be seen from Figures 7b and 9 that when the texture is perpendicular to the friction direction, as the contact angle increases, the COF and wear volume increase gradually, but the increase is very small. When the texture is parallel to the friction direction, as the contact angle increases, the COF increases, but the wear volume decreases. The texture perpendicular to the friction direction was more conducive to the preparation of parts that required a small COF and a large wear volume, such as cheap parts that were easy to replace, and which would protect other high-precision and expensive parts. The texture parallel to the friction direction was more conducive to the preparation of situations that required a large COF and small wear volume, such as parts that were not easy to replace or that were expensive.

5. Conclusions

We used a nanosecond pulsed laser to realize the preparation of the superhydrophobic nickel surface and we studied the friction and wear properties of the superhydrophobic nickel surface with different contact angles under dry friction conditions. Compared to the unprocessed surface, the laser-fabricated superhydrophobic surface reduced the friction coefficient of nickel but also increased the wear volume. However, as the contact angle increased, the COF of the superhydrophobic surface increased gradually and the wear volume decreased gradually. The texture perpendicular to the friction direction is more conducive to the preparation of parts requiring a small COF and large wear volume, while the texture parallel to the friction direction is more conducive to the preparation of parts requiring a large COF and small wear volume. This method provides a reference for preparing superhydrophobic surfaces with more suitable friction and wear properties.

Author Contributions: Conceptualization, J.H. and Z.Z.; methodology, J.H.; software, D.G.; validation, Z.Z. and D.G.; formal analysis, Z.N.; investigation, J.H.; resources, L.Z.; data curation, D.G.; writing—original draft preparation, J.H.; writing—review and editing, J.H.; visualization, W.Z.; supervision, L.Z.; project administration, W.Z.; funding acquisition, L.Z. and W.Z. All authors have read and agreed to the published version of the manuscript.

Funding: National Natural Science Foundation of China (51975036).

Institutional Review Board Statement: Not applicable.

Informed Consent Statement: Not applicable.

Data Availability Statement: Not applicable.

Conflicts of Interest: The authors declare no conflict of interest.

References

1. Kung, C.H.; Sow, P.K.; Zahiri, B.; Mérida, W. Assessment and Interpretation of Surface Wettability Based on Sessile Droplet Contact Angle Measurement: Challenges and Opportunities. *Adv. Mater. Interfaces* **2019**, *6*, 1900839. [[CrossRef](#)]
2. Sharma, A.; Arora, H.; Grewal, H.S. Self-regenerative superhydrophobic metallic coatings with enhanced durability. *Surf. Coatings Technol.* **2023**, *462*, 129459. [[CrossRef](#)]
3. Ding, K.; Wang, C.; Li, S.; Zhang, X.; Lin, N. Large-area cactus-like micro-/nanostructures with anti-reflection and superhydrophobicity fabricated by femtosecond laser and thermal treatment. *Surf. Interfaces* **2022**, *33*, 102292. [[CrossRef](#)]
4. Feng, X.; Sun, P.; Tian, G. Recent Developments of Superhydrophobic Surfaces (SHS) for Underwater Drag Reduction Opportunities and Challenges. *Adv. Mater. Interfaces* **2021**, *9*, 2101616. [[CrossRef](#)]
5. Lan, X.; Zhang, B.; Wang, J.; Fan, X.; Zhang, J. Hydrothermally structured superhydrophobic surface with superior anti-corrosion, anti-bacterial and anti-icing behaviors. *Colloids Surfaces A Physicochem. Eng. Asp.* **2021**, *624*, 126820. [[CrossRef](#)]
6. Liravi, M.; Pakzad, H.; Moosavi, A.; Nouri-Borujerdi, A. A comprehensive review on recent advances in superhydrophobic surfaces and their applications for drag reduction. *Prog. Org. Coat.* **2020**, *140*, 105537. [[CrossRef](#)]
7. Wang, C.X.; Zhang, X.F. A non-particle and fluorine-free superhydrophobic surface based on one-step electrodeposition of dodecyltrimethoxysilane on mild steel for corrosion protection. *Corros. Sci.* **2020**, *163*, 108284. [[CrossRef](#)]
8. Song, Y.; Wang, C.; Dong, X.; Yin, K.; Zhang, F.; Xie, Z.; Chu, D.; Duan, J. Controllable superhydrophobic aluminum surfaces with tunable adhesion fabricated by femtosecond laser. *Opt. Laser Technol.* **2018**, *102*, 25–31. [[CrossRef](#)]
9. Liu, Y.; Li, S.; Niu, S.; Cao, X.; Han, Z.; Ren, L. Bio-inspired micro-nano structured surface with structural color and anisotropic wettability on Cu substrate. *Appl. Surf. Sci.* **2016**, *379*, 230–237. [[CrossRef](#)]
10. Rajab, F.H.; Liu, Z.; Li, L. Long term superhydrophobic and hybrid superhydrophobic/superhydrophilic surfaces produced by laser surface micro/nano surface structuring. *Appl. Surf. Sci.* **2018**, *466*, 808–821. [[CrossRef](#)]
11. Huang, W.; Ordikhani-Seyedlar, R.; Samanta, A.; Shaw, S.; Ding, H. Quantification of superhydrophobic functionalization for laser textured metal surfaces. *Colloids Surf. A Physicochem. Eng. Asp.* **2022**, *636*, 128126. [[CrossRef](#)]
12. Lu, Y.; Guan, Y.; Li, Y.; Yang, L.; Wang, M.; Wang, Y. Nanosecond laser fabrication of superhydrophobic surface on 316L stainless steel and corrosion protection application. *Colloids Surfaces A Physicochem. Eng. Asp.* **2020**, *604*, 125259. [[CrossRef](#)]
13. Huang, J.; Yang, S. Investigation on anisotropic tribological properties of superhydrophobic/superlipophilic lead bronze surface textured by femtosecond laser. *Appl. Surf. Sci.* **2021**, *579*, 152223. [[CrossRef](#)]
14. Shimada, H.; Kato, S.; Watanabe, T.; Yamaguchi, M. Direct laser processing of two-scale periodic structures for superhydrophobic surfaces using a nanosecond pulsed laser. *Lasers Manuf. Mater. Process.* **2020**, *7*, 496–512. [[CrossRef](#)]
15. He, Y.; Wang, L.; Wu, T.; Wu, Z.; Chen, Y.; Yin, K. Facile fabrication of hierarchical textures for substrate-independent and durable superhydrophobic surfaces. *Nanoscale* **2022**, *14*, 9392–9400. [[CrossRef](#)]

16. Han, X.; Ren, L.; Ma, Y.; Gong, X.; Wang, H. A mussel-inspired self-repairing superhydrophobic coating with good anti-corrosion and photothermal properties. *Carbon* **2022**, *197*, 27–39. [[CrossRef](#)]
17. Li, H.; Luo, Y.; Yu, F.; Zhang, H. In-situ construction of MOFs-based superhydrophobic/superoleophilic coating on filter paper with self-cleaning and antibacterial activity for efficient oil/water separation. *Colloids Surfaces A Physicochem. Eng. Asp.* **2021**, *625*, 126976. [[CrossRef](#)]
18. Jiao, Y.; Zhang, T.; Ji, J.; Guo, Y.; Wang, Z.; Tao, T.; Xu, J.; Liu, X.; Liu, K. Functional Microtextured Superhydrophobic Surface with Excellent Anti-Wear Resistance and Friction Reduction Properties. *Langmuir* **2022**, *38*, 13166–13176. [[CrossRef](#)] [[PubMed](#)]
19. Guo, Y.; Zhang, X.; Wang, X.; Xu, Q.; Geng, T. Wetting and tribological properties of superhydrophobic aluminum surfaces with different water adhesion. *J. Mater. Sci.* **2020**, *55*, 11658–11668. [[CrossRef](#)]
20. Huang, J.; Wei, S.; Zhang, L.; Yang, Y.; Yang, S.; Shen, Z. Fabricating the Superhydrophobic Nickel and Improving Its Antifriction Performance by the Laser Surface Texturing. *Materials* **2019**, *12*, 1155. [[CrossRef](#)]
21. Kasman, Ş.; Uçar, I.C.; Ozan, S. Investigation of laser surface texturing parameters of biomedical grade Co-Cr-Mo alloy. *Int. J. Adv. Manuf. Technol.* **2023**, *125*, 4271–4291. [[CrossRef](#)]
22. Ahangaran, F.; Navarchian, A.H. Recent advances in chemical surface modification of metal oxide nanoparticles with silane coupling agents: A review. *Adv. Colloid Interface Sci.* **2020**, *286*, 102298. [[CrossRef](#)] [[PubMed](#)]
23. Allahdini, A.; Jafari, R.; Momen, G. Transparent non-fluorinated superhydrophobic coating with enhanced anti-icing performance. *Prog. Org. Coatings* **2022**, *165*, 106758. [[CrossRef](#)]
24. Guan, Y.; Cui, X.; Chen, D.; Su, W.; Zhao, Y.; Li, J.; Feng, L.; Li, X.; Jin, G. Realizing excellent tribological properties of BCC/FCC gradient high -entropy alloy coating via an in-situ interface reaction. *Mater. Today Commun.* **2023**, *35*, 106098. [[CrossRef](#)]
25. Huang, J.; Guan, Y.; Ramakrishna, S. Tribological behavior of femtosecond laser-textured leaded brass. *Tribol. Int.* **2021**, *162*, 107115. [[CrossRef](#)]

Disclaimer/Publisher's Note: The statements, opinions and data contained in all publications are solely those of the individual author(s) and contributor(s) and not of MDPI and/or the editor(s). MDPI and/or the editor(s) disclaim responsibility for any injury to people or property resulting from any ideas, methods, instructions or products referred to in the content.